Ecotoxicology (2015) 24:2067–2072
DOI 10.1007/s10646-015-1554-1

Morphology-dependent antimicrobial activity of Cu/Cu_xO nanoparticles

Lu Xiong[1] · Zhong-Hua Tong[1] · Jie-Jie Chen[1] · Ling-Li Li[1] · Han-Qing Yu[1]

Accepted: 16 September 2015 / Published online: 25 September 2015

Abstract Cu/Cu_xO nanoparticles (NPs) with different morphologies have been synthesized with glucose as a reducing agent. The X-ray diffraction and Scanning electron microscopy imaging show that the Cu/Cu_xO NPs have fine crystalline peaks with homogeneous polyhedral, flower-like, and thumbtack-like morphologies. Their antimicrobial activities were evaluated on inactivation of *Escherichia coli* using a fluorescence-based live/dead staining method. Dissolution of copper ions from these NPs was determined. Results demonstrated a significant growth inhibition for these NPs with different morphologies, and the flower-like Cu/Cu_xO NPs were the most effective form, where more copper ions were dissolved into the culture media. Surface free energy calculations based on first-principle density functional theory show that different crystal facets of the copper NPs have diverse surface energy, indicating the highest reactivity of the flower-like NPs, which is consistent with the results from the dissolution study and antimicrobial activity test. Together, these results suggest that the difference between the surface free energy may be a cause for their morphology-dependent antimicrobial activity.

Keywords Copper nanoparticles · Morphology · Antimicrobial activity · Surface free energy

✉ Zhong-Hua Tong
zhtong@ustc.edu.cn

[1] CAS Key Laboratory of Urban Pollutant Conversion, Department of Chemistry, University of Science & Technology of China, Hefei 230026, China

Introduction

Metal nanoparticles (NPs) have received considerable attention for their unique properties, including optical, catalytic, electrical, magnetic and biological activities (Hirsch et al. 2003; Gyawali et al. 2011). It has been demonstrated that metal NPs exhibit a wide spectrum of antimicrobial activity against bacteria, fungi and viruses (Stoimenov et al. 2002). Copper has been a good choice to work with, because it is less expensive and shares properties similar to noble metals, such as silver and gold. With the development of nanotechnology, copper oxide NPs are among the most widely applied antimicrobial materials for their high efficacy toward a broad spectrum of microorganisms (Borkow et al. 2010; Liu et al. 2014).

Copper oxide NPs can be prepared using different methods, such as solution based method assisted with templates (Hsieh et al. 2003), hydrothermal method (Gao and Liu 2015), electrochemical methods (Ben Salem et al. 2014), and thermal oxidation method (Li et al. 2013). Different sized NPs can be obtained by adjusting growth parameters during synthesis (Chen et al. 2015) or with post-synthesis separation such as centrifugation and ultrasonication (Sun et al. 2009). Recent studies have observed that differences in particle size can alter antimicrobial activity against bacterial growth (Azam et al. 2012; Adams et al. 2014). The antimicrobial activity of the NPs can also be governed by chemical composition, surface charge, morphology and experimental conditions (Simon-Deckers et al. 2009; Nesic et al. 2014; Theja et al. 2014). Studies on the antimicrobial activity of metallic NPs have reported the generation of reactive oxygen species (ROS) and their corresponding ions from NPs, which subsequently result in oxidative damage to cellular structures (Gunawan et al. 2011; Applerot et al. 2012). Although there are a few

probable modes of bacteria-nanoparticle interaction, the mechanisms behind the antimicrobial activity are not yet fully understood.

This work is aimed to find out how the antimicrobial activity of copper NPs is related to their morphology. Three different morphologies of copper NPs were synthesized. Their effects on bacterial growth and dissolution of copper ions were determined. The first principle calculations based on density functional theory (DFT) were applied to provide molecular level insights into morphology effects. Results from our study may provide a new strategy for improving the antimicrobial efficacy of nanoparticles.

Materials and methods

Cu/Cu_xO nanoparticle synthesis and characterization

All chemical reagents were of analytical grade and used as received. Cu/Cu_xO NPs with different morphologies were prepared using glucose as a reducing agent by modification of a previously reported method (Jin et al. 2011). Polyhedral nanostructures were prepared by mixing $CuCl_2{\cdot}2H_2O$ (20 mg), glucose (50 mg) and polyvinylpyrrolidone (PVP, 20 mg) with 10 mL of water at 50 °C for 3 h. Then 10 mg of NaOH was added, and the reduction reaction was performed at 90 °C for 2 h. Thumbtack-like nanostructures were prepared similarly, except that more $CuCl_2{\cdot}2H_2O$ (40 mg) and KBr (20 mg) were added to the water in the first step. Flower-like nanostructures were prepared by adding more glucose (100 mg) and using cetyl trimethyl ammonium bromide (CTAB) instead of PVP in the first step, and the obtained particles after the reduction reaction were re-suspended in 10 mL of water amended with KOH (10 mg), KBr (10 mg) and PVP (10 mg), and then mixed at 50 °C for 2 h. Finally, the particle samples with different morphology were washed with distilled water and ethanol for three times. The morphology and size of the NPs were characterized by scanning electron microscope (SEM) (Supra 40, Zeiss Co., Germany). Powder X-ray diffraction (XRD) (X'Pert, PANalytical BV, the Netherlands) was used to analyze the crystal structure.

Antimicrobial evaluation on *E. coli* proliferation

E. coli JM109 from a single agar plate colony was cultured overnight in Lurial-Bertani medium (LB; 5 g yeast extract, 10 g tryptone, 5 g NaCl per liter) at 30 °C with shaking under dark condition. One mL of the overnight culture was transferred into 20 mL of fresh LB. For each growth experiment, 6 mg of dry-state Cu/Cu_xO NPs was added into 20 mL of LB with bacterial inoculum and cultured at 30 °C for 6 h with shaking along with an untreated control. To avoid disturbance of suspended particles on optical density measurement of cell concentration, a fluorescence-based assay was used to determine the antimicrobial effects of Cu/Cu_xO NPs.

The amount of bacteria cells were estimated based on the rationale that 4-6-diamidino-2-phenylindole (DAPI) stains both live and dead bacteria, while propidium iodide (PI) is able to penetrate only damaged or dead cells. *E. coli* cells were stained with PI (20 μg/mL) for 20 min, and counter-stained with DAPI (10 μg/mL) for 15 min in the dark. After staining, *E. coli* cells were centrifuged for dye removal and resuspended in 20 mL of 50 mM phosphate buffer. Then 10 μL of the solution was added onto a glass slide followed by a coverslip, and observed with a confocal laser scanning micro scopy (CLSM) (FV1000-IX81, Olympus, Japan). A minimum of 5 fields were examined for each plate to estimate the number of viable cells. Dissolution of copper ions from 300 mg/L of copper NPs in LB medium was determined with inductively coupled plasma atomic emission spectroscopy (ICP-AES) (Optima 7300 DV, Perkin Elmer Co., USA). The experiments were conducted in triplicate. Results were statistically analyzed by one-way analysis of variance (ANOVA) followed by Tukey's test for comparing treatment effects at $\alpha = 0.05$. A P value of <0.05 was considered statistically significant.

Theoretical calculations

First-principle DFT calculation were performed based on the generalized gradient approximation (GGA) with plane-wave basis sets and ultrasoft pseudopotentials (Vanderbilt 1990), as implemented in the CASTEP module (Segall et al. 2002) of Materials Studio. The geometries of (111), (200), and (220) surfaces of Cu_2O and Cu were optimized and the total energies were obtained. The exchange–correlation energy and potential were described self-consistently using the Perdew, Burke, and Ernzerhof (PBE) functional (Perdew et al. 1996). The *Express* quality setting, which has been widely used to study semiconductors, insulators and nonmagnetic metals with good accuracy, was employed to attain a compromise between speed and accuracy. Here, the tolerance of the energy was set as 1×10^{-3} eV/cell. This setting is an order of magnitude faster than the *Fine* setting, so that the produced results could be sufficiently accurate for exploratory studies. Brillouin zone integration was performed with variable number of k-points generated by Monkhorst–Pack algorithm, depending on the unit cell size and shape (Monkhorst and Pack 1976).

Results and discussion

Structural properties Cu/Cu_xO NPs

Copper NPs were synthesized using glucose as a reducing agent, water as a solvent, and four different capping agents, through a hydrothermal method. The structural features of the particles were investigated by powder XRD. As shown in Fig. 1a, c, the diffraction peaks can be indexed as cuprous oxide phase (JCPDS no. 05-0667) (Liu et al. 2012), while the diffraction peaks in Fig. 1b represent the crystal facets of metal copper phase (JCPDS no. 85-1326) (Yin et al. 2005). The higher (111) diffraction intensity of these copper NPs suggests that the produced NPs have {111} crystal planes, as reported in other study (Lee et al. 2011).

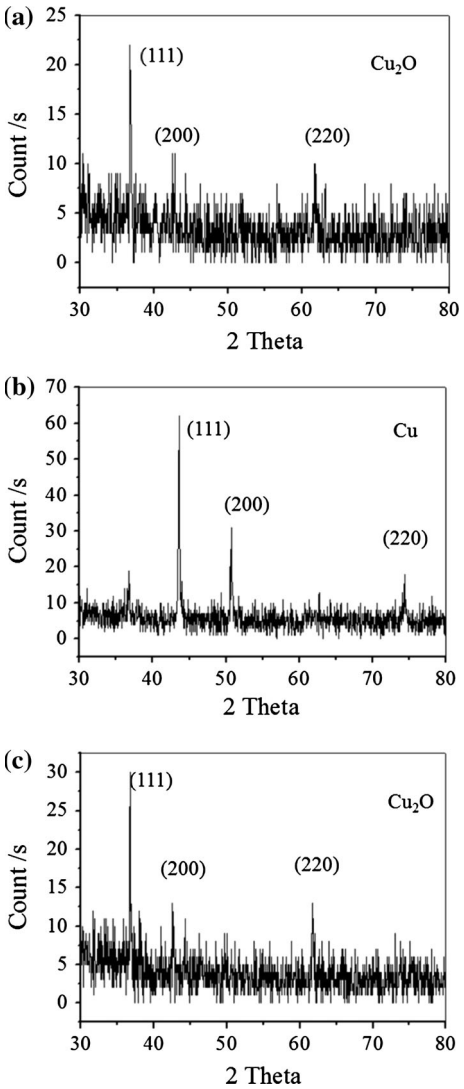

Fig. 1 XRD of polyhedral (**a**), flower-like (**b**) and thumbtack-like (**c**) copper nanoparticles

The morphology and size of the produced particles were characterized with SEM. Three types of copper NPs were prepared showing polyhedral, flower- and thumbtack-like nanostructures with fine crystalline morphologies (Fig. 2). The sizes of the polyhedral particles were measured to be around 400 nm. The sizes of the flower- and thumbtack-like particles were smaller.

Antimicrobial activity of Cu/Cu_xO NPs and leaching of copper ions

The antibacterial actions of the produced Cu/Cu_xO NPs were evaluated against the growth of model bacteria

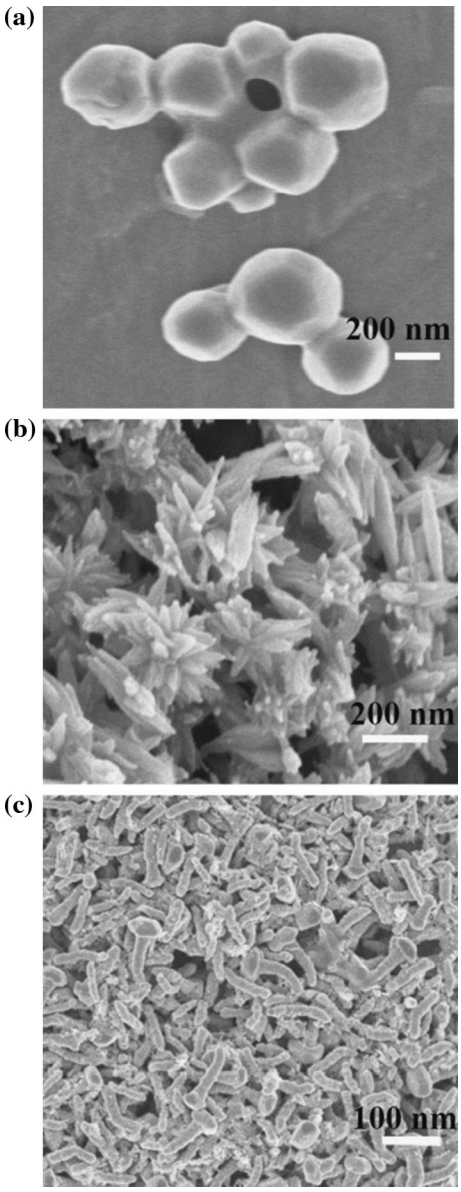

Fig. 2 SEM image of polyhedral (**a**), flower-like (**b**) and thumbtack-like (**c**) copper nanoparticles

E. coli. After 6 h exposure, the biomass of *E. coli* was determined using DAPI staining which has been widely used to quantify the gross cell number (Haglund et al. 2003). At the same time, dead bacterial biomass was determined using PI (Foladori et al. 2010). Figure 3a–d show the bacterial biomass in the presence of homogeneously dispersed Cu/Cu_xO NPs at a dosage of 300 mg/L. Compared with the untreated control, the growth of *E. coli* was significantly inhibited following the application of Cu/Cu_xO NPs ($P < 0.05$). The bacterial biomass was inhibited by 80–94 % with respect to the untreated control. The extent of inhibition of bacterial growth observed in this study was found to be significantly associated with the shapes of the particles ($P < 0.05$), and the flower-like copper NPs were the most effective morphology. This morphology-dependent antibacterial activity has been previously demonstrated in other particles (Wang et al. 2010; Talebian et al. 2013).

Corresponding to the growth inhibition experiment, dissolution of copper ions in LB medium was carried out for 6 h. As shown in Fig. 4, leaching of soluble copper proceeded rapidly within the first hour, with >80 % of the total soluble copper measured in the culture medium with different Cu/Cu_xO NPs exposure. A higher ($P > 0.05$) dissolution of 87 % was observed for the flower-like nanostructure in the first hour. Equilibrium was reached after 3 h for all morphologies, with the highest ($P > 0.05$) total soluble Cu concentration at 206 mg/L for the flower-like nanostructure. Dissolution of metal ions from various metal oxide NPs have been previously reported (Elzey and Grassian 2010; Odzak et al. 2014), which affects the abundance, uptake and toxicity mechanisms of NPs (Misra et al. 2012).

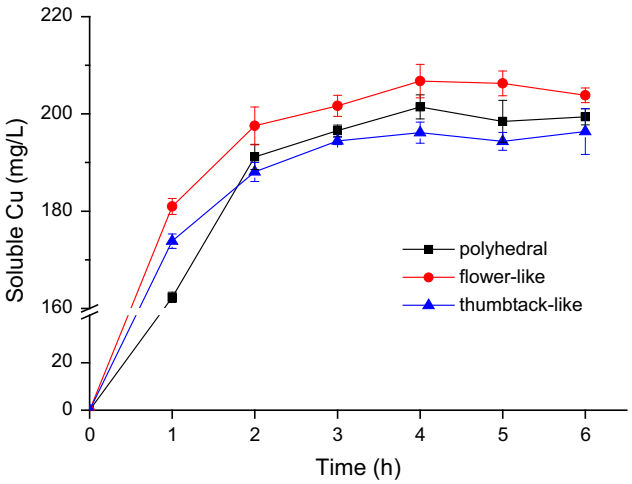

Fig. 4 Dissolution of Cu with time in LB medium. Data are expressed as mean ± SD, n = 3. The test shows faster dissolution of copper ions from the flower-like Cu/Cu_xO NPs ($P < 0.05$)

DFT calculations

Previously studies have support the concept that the morphology of particles is closely associated with the antibacterial activity (Simon-Deckers et al. 2009; Wang et al. 2010; Talebian et al. 2013). However, detailed mechanisms for the morphology-dependent antibacterial activity of these particles remain to be determined. Studies show that morphology-dependent catalytic effect can be

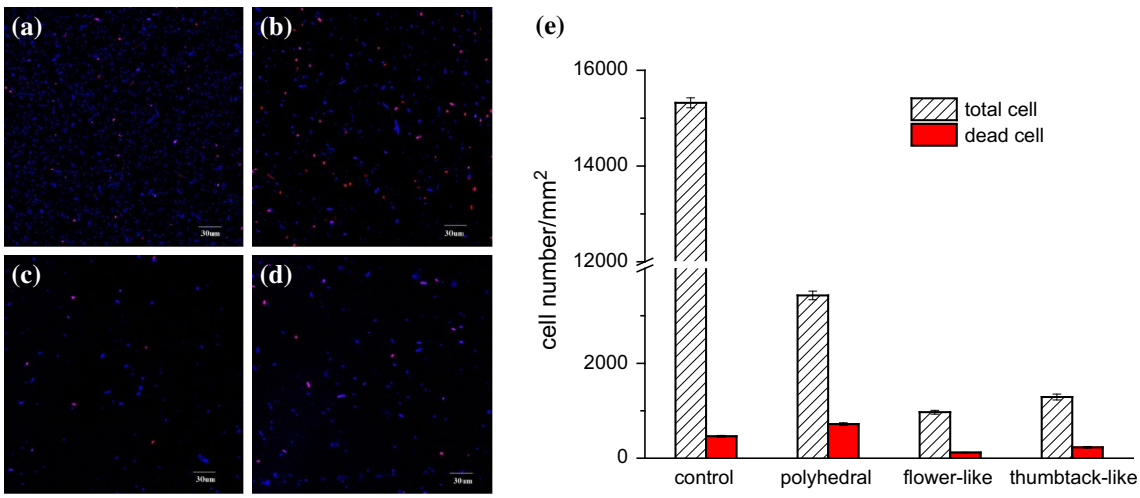

Fig. 3 Fluorescence microscope images of bacterial cells for (**a**) control sample and samples exposed to (**b**) polyhedral, (**c**) flower-like and (**d**) thumbtack-like Cu/Cu_xO NPs (total cells stained with DAPI, dead cells stained with PI). (**e**) Fluorescence-based assay showing the antimicrobial activity of copper NPs. Data are expressed as mean ± SD, n = 3. The test confirms decreased viable cells with Cu/Cu_xO NPs relative to the control with $P < 0.05$

attributed to surface active sites of different structural features (Liu et al. 2008; Gao et al. 2013). Therefore, surface energy calculations based on DFT theory were performed for a preliminary investigation of their mechanism of action.

Surface free energy (γ) was calculated according to the following equation:

$$= \frac{E^{slab} - NE^{bulk}}{2A}$$

where E^{bulk} is the energy per unit of Cu or Cu_2O, E^{slab} is the total energy of the slab, N is the total number of unit Cu or Cu_2O contained in the slab model. According to the above equation, the value of $\gamma_{Cu2O(111)}$ was -94 eV/Å^2, $\gamma_{Cu2O(220)} = 0.05$ eV/Å^2,$\gamma_{Cu2O(200)} = 0.07$ eV/Å^2. For Cu, $\gamma_{Cu(111)} = 238$ eV/Å^2, $\gamma_{Cu(200)} = 206$ eV/Å^2, $\gamma_{Cu(221)} = 146$ eV/Å^2. So the surface free energy was in an order as $\gamma Cu(111) > \gamma Cu(200) > \gamma Cu(220) > \gamma Cu_2O(200) > \gamma Cu_2O(220) > \gamma Cu_2O(111)$. Combined with the XRD analysis, these results show that the main exposed facets {111} of the flower-like crystrals have a much higher surface energy than the main exposed facets {111} of the polyhedral and thumbtack-like crystals. Higher surface energy of the exposed facets might be more efficient in generating toxic copper ions (Pang et al. 2009), which could result in higher antibacterial activity of the flower-like crystals. As for the polyhedral and thumbtack-like crystals, they share the same exposed facets. The difference in their antibacterial activity might be attributed to the much smaller size of the thumbtack-like crystals (Azam et al. 2012).

Several mechanisms have been proposed to explain the antimicrobial activity of nanostructure materials, such as generation of reactive oxygen species (ROS), physical damage, and release of metal ions. The induction of ROS after exposure to nanomaterials has been demonstrated in numerous studies, leading to disruption of cell wall, DNA damage, and subsequently cell death (Choi and Hu 2008; Rupareli et al. 2008). Physical damage has been shown as an effective mechanism in bacterial inactivation. Akhavan and Ghaderi (2010) demonstrated that the bacterial cell membrane was damaged by interacting with the extremely sharp edges of the nanowalls. Binding of nano-silica silver nanocomposite on bacterial cell walls have been shown to cause loss of cell membrane integrity and efflux of cytoplasmic materials (Parandhaman et al. 2015). Release of soluble ions from nano-sized metal oxide has been proposed as an important mechanism of action (Gunawan et al. 2011; Misra et al. 2012). Formation of ROS was also found to be related with crystalline nature of nano-metal oxides (Perelshtein et al. 2015). Therefore, these mechanisms may not work separately suggesting that more than one factor would contribute simultaneously to the antimicrobial action.

Conclusions

In this study, polyhedral, flower-like and thumbtack-like Cu/Cu_xO NPs were synthesized through a hydrothermal method with glucose as a reducing agent. Structural property of the copper NPs was examined by XRD and SEM, showing that the Cu/Cu_xO NPs have fine crystal structures. The antibacterial activity of the Cu/Cu_xO NPs against *E. coli* was examined using a fluorescence-based live/dead staining method. Dissolution of copper ions from these NPs was determined with ICP-AES. Results show that the flower-like Cu/Cu_xO NPs were the most effective morphology and more copper ions were dissolved into the culture media. The mechanism of morphology-dependent antibacterial activity was discussed based on surface energy calculation for the exposure facets of the produced nanocrystals.

Acknowledgments The authors wish to thank the NSFC (21477121), Hefei Center for Physical Science and Technology (2014FXCX010), the Program for Changjiang Scholars and Innovative Research Team in University, and Innovation Center of Suzhou Nano Science and Technology for the partial support of this study.

Compliance with ethical standards

Conflict of interest All authors declare that they have no conflict of interest.

References

Adams CP, Walker KA, Obare SO, Docherty KM (2014) Size-dependent antimicrobial effects of novel palladium nanoparticles. PLoS ONE 9:e85981

Akhavan O, Ghaderi E (2010) Toxicity of graphene and graphene oxide nanowalls against bacteria. ACS Nano 4:5731–5736

Applerot G, Lellouche J, Lipovsky A, Nitzan Y, Lubart R, Gedanken A, Banin E (2012) Understanding the antibacterial mechanism of CuO nanoparticles: revealing the route of induced oxidative stress. Small 8:3326–3337

Azam A, Ahmed AS, Oves M, Khan MS, Memic A (2012) Size-dependent antimicrobial properties of CuO nanoparticles against gram-positive and -negative bacterial strains. Int J Nanomed 7:3527–3535

Ben Salem S, Ben Achour Z, Thamri K, Touayar O (2014) Study and characterization of porous copper oxide produced by electrochemical anodization for radiometric heat absorber. Nanoscale Res Lett 9:577

Borkow G, Zhou SS, Page T, Gabbay JA (2010) Novel anti-influenza copper oxide containing respiratory face mask. PLoS ONE 5:e11295

Chen S, Su HY, Wang YC, Wu WL, Zeng J (2015) Size-controlled synthesis of platinum-copper hierarchical trigonal bipyramid nanoframes. Angew Chem-Int Ed 54:108–113

Choi O, Hu ZQ (2008) Size dependent and reactive oxygen species related nanosilver toxicity to nitrifying bacteria. Environ Sci Technol 42:4583–4588

Elzey S, Grassian VH (2010) Nanoparticle dissolution from the particle perspective: insights from particle sizing measurements. Langmuir 26:12505–12508

Foladori P, Bruni L, Tamburini S, Ziglio G (2010) Direct quantification of bacterial biomass in influent, effluent and activated sludge of wastewater treatment plants by using flow cytometry. Water Res 44:3807–3818

Gao P, Liu DW (2015) Facile synthesis of copper oxide nanostructures and their application in non-enzymatic hydrogen peroxide sensing. Sens Actuator B-Chem 208:346–354

Gao RH, Zhang DS, Maitarad P, Shi LY, Rungrotmongkol T, Li HR, Zhang JP, Cao WG (2013) Morphology-dependent properties of MnO_x/ZrO_2 CeO_2 nanostructures for the selective catalytic reduction of NO with NH_3. J Phys Chem C 117:10502–10511

Gunawan C, Teoh WY, Marquis CP, Amal R (2011) Cytotoxic origin of copper(II) oxide nanoparticles: comparative studies with micron-sized particles, leachate, and metal salts. ACS Nano 5:7214–7225

Gyawali R, Ibrahim SA, Abu Hasfa SH, Smqadri SQ, Haik Y (2011) Antimicrobial activity of copper alone and in combination with lactic acid against *Escherichia coli* O157:H7 in laboratory medium and on the surface of lettuce and tomatoes. J Pathog 2011:650968

Haglund AL, Lantz P, Tornblom E, Tranvik L (2003) Depth distribution of active bacteria and bacterial activity in lake sediment. FEMS Microbiol Ecol 46:31–38

Hirsch LR, Stafford RJ, Bankson JA, Sershen SR, Rivera B, Price RE, Hazle JD, Halas NJ, West JL (2003) Nanoshell-mediated near-infrared thermal therapy of tumors under magnetic resonance guidance. Proc Natl Acad Sci USA 100:13549–13554

Hsieh CT, Chen JM, Lin HH, Shih HC (2003) Synthesis of well-ordered CuO nanofibers by a self-catalytic growth mechanism. Appl Phys Lett 82:3316–3318

Jin MS, He GN, Zhang H, Zeng J, Xie ZX, Xia YN (2011) Shape-controlled synthesis of copper nanocrystals in an aqueous solution with glucose as a reducing agent and hexadecylamine as a capping agent. Angew Chem Int Ed 50:10560–10564

Lee SK, Liang CW, Martin LW (2011) Synthesis, control, and characterization of surface properties of Cu_2O nanostructures. ACS Nano 5:3736–3743

Li X, Liang J, Kishi N, Soga T (2013) Synthesis of cupric oxide nanowires on spherical surface by thermal oxidation method. Mater Lett 96:192–194

Liu L, Liu HJ, Zhao YP, Wang YQ, Duan YQ, Gao GD, Ge M, Chen W (2008) Directed synthesis of hierarchical nanostructured TiO_2 catalysts and their morphology-dependent photocatalysis for phenol degradation. Environ Sci Technol 42:2342–2348

Liu GG, He F, Li XQ, Wang SH, Li LJ, Zuo GF, Huang Y, Wan YZ (2012) Three-dimensional cuprous oxide microtube lattices with high catalytic activity templated by bacterial cellulose nanofibers. J Mater Chem 21:10637–10640

Liu C, Xie X, Zhao WT, Yao J, Kong DS, Boehm AB, Cui Y (2014) Static electricity powered copper oxide nanowire microbicidal electroporation for water disinfection. Nano Lett 14:5603–5608

Misra SK, Dybowska A, Berhanu D, Luoma SN, Valsami-Jones E (2012) The complexity of nanoparticle dissolution and its importance in nanotoxicological studies. Sci Total Environ 438:225–232

Monkhorst HJ, Pack JD (1976) Special points for brillouin-zone integrations. Phys Rev B 13:5188–5192

Nesic J, Rtimi S, Laub D, Roglic GM, Pulgarin C, Kiwi J (2014) New evidence for TiO_2 uniform surfaces leading to complete bacterial reduction in the dark: critical issues. Colloid Surf B-Biointerfaces 123:593–599

Odzak N, Kistler D, Behra R, Sigg L (2014) Dissolution of metal and metal oxide nanoparticles in aqueous media. Environ Pollut 191:132–138

Pang H, Gao F, Lu QY (2009) Morphology effect on antibacterial activity of cuprous oxide. Chem Commun 9:1076–1078

Parandhaman T, Das A, Ramalingam B, Samanta D, Sastry TP, Mandal AB, Das SK (2015) Antimicrobial behavior of biosynthesized silica-silver nanocomposite for water disinfection: a mechanistic perspective. J Hazard Mater 290:117–126

Perdew JP, Burke K, Ernzerhof M (1996) Generalized gradient approximation made simple. Phys Rev Lett 77:3865–3868

Perelshtein I, Lipovsky A, Perkas N, Gedanken A, Moschini E, Mantecca P (2015) The influence of the crystalline nature of nano-metal oxides on their antibacterial and toxicity properties. NANO Res 8:695–707

Rupareli JP, Chatterjee AK, Duttagupta SP, Mukherji S (2008) Strain specificity in antimicrobial activity of silver and copper nanoparticles. Acta Biomater 4:707–771

Segall MD, Lindan PJD, Probert MJ, Pickard CJ, Hasnip PJ, Clark SJ, Payne MC (2002) First-principles simulation: ideas, illustrations and the CASTEP code. J Phys- Condens Matter 14:2717–2744

Simon-Deckers A, Loo S, Mayne-L'Hermite M, Herlin-Boime N, Menguy N, Reynaud C, Gouget B, Carriere M (2009) Size-, composition- and shape-dependent toxicological impact of metal oxide nanoparticles and carbon nanotubes toward bacteria. Environ Sci Technol 43:8423–8429

Stoimenov PK, Klinger RL, Marchin GL, Klabunde KJ (2002) Metal oxide nanoparticles as bactericidal agents. Langmuir 18: 6679–6686

Sun XM, Tabakman SM, Seo WS, Zhang L, Zhang GY, Sherlock S, Bai L, Dai HJ (2009) Separation of nanoparticles in a density gradient: FeCo@C and gold nanocrystals. Angew Chem-Int Ed 48:939–942

Talebian N, Amininezhad SM, Doudi M (2013) Controllable synthesis of ZnO nanoparticles and their morphology-dependent antibacterial and optical properties. J Photochem Photobiol B-Biol 120:66–73

Theja GS, Lowrence RC, Ravi V, Nagarajan S, Anthony SP (2014) Synthesis of Cu_2O micro/nanocrystals with tunable morphologies using coordinating ligands as structure controlling agents and antimicrobial studies. CrystEngComm 16:9866–9872

Vanderbilt D (1990) Soft self-consistent pseudopotentials in a generalized eigenvalue formalism. Phys Rev B 41:7892–7895

Wang X, Wu HF, Kuang Q, Huang RB, Xie ZX, Zheng LS (2010) Shape-dependent antibacterial activities of Ag_2O polyhedral particles. Langmuir 26:2774–2778

Yin M, Wu CK, Lou YB, Burda C, Koberstein JT, Zhu YM, O'Brien S (2005) Copper oxide nanocrystals. J Am Chem Soc 127:9506–9544